


ANNALS OF THE NEW YORK ACADEMY OF SCIENCES

Special Issue: *Musculoskeletal Repair and Regeneration*

ORIGINAL ARTICLE

Polymeric mesh and insulin-like growth factor 1 delivery enhance cell homing and graft–cartilage integration

Margaret K. Boushell,¹ Christopher Z. Mosher,² Gurbani K. Suri,¹ Stephen B. Doty,² Eric J. Strauss,³ Ernst B. Hunziker,⁴ and Helen H. Lu ¹

¹Biomaterials and Interface Tissue Engineering Laboratory, Department of Biomedical Engineering, Columbia University, New York, New York. ²Analytical Microscopy Laboratory, Hospital for Special Surgery, New York, New York. ³Department of Orthopaedic Surgery, NYU Langone Medical Center, New York, New York. ⁴Department of BioMedical Research, University Hospital of Bern, University of Bern, Bern, Switzerland

Address for correspondence: Helen H. Lu, Department of Biomedical Engineering, Columbia University, 1210 Amsterdam Avenue, 351 Engineering Terrace, MC 8904, New York, NY 10027. hllu@columbia.edu

Cartilage injury, such as full-thickness lesions, predisposes patients to the premature development of osteoarthritis, a degenerative joint disease. While surgical management of cartilage lesions has improved, long-term clinical efficacy has stagnated, owing to the lack of hyaline cartilage regeneration and inadequate graft–host integration. This study tests the hypothesis that integration of cartilage grafts with native cartilage can be improved by enhancing the migration of chondrocytes across the graft–host interface via the release of chemotactic factor from a degradable polymeric mesh. To this end, a polylactide-*co*-glycolide/poly- ϵ -caprolactone mesh was designed to localize the delivery of insulin-like growth factor 1 (IGF-1), a well-established chondrocyte attractant. The release of IGF-1 (100 ng/mg) enhanced cell migration from cartilage explants, and the mesh served as critical structural support for cell adhesion, growth, and production of a cartilaginous matrix *in vitro*, which resulted in increased integration strength compared with mesh-free repair. Further, this neocartilage matrix was structurally contiguous with native and grafted cartilage when tested in an osteochondral explant model *in vivo*. These results demonstrate that this combined approach of a cell homing factor and supportive matrix will promote cell-mediated integrative cartilage repair and improve clinical outcomes of cartilage grafts in the treatment of osteoarthritis.

Keywords: cartilage; IGF-1; chondrocyte; interface; chemotaxis; electrospinning

Introduction

Osteoarthritis (OA) is characterized by progressive articular cartilage lesions and afflicts nearly 30 million Americans, with an increasing prevalence in the aging population.¹ Epidemiologic reviews of consecutive knee arthroscopies revealed that the incidence of full-thickness cartilage defects is around 60–65% in such patients, irrespective of the surgical indication.^{2,3} Secondary to nonphysiological stress distribution, this extent of cartilage lesions predisposes patients to OA.⁴ Articular cartilage defects greater than 1 cm² in size significantly increase and concentrate contact stresses on both the defect rim and the opposing articular surface, potentially inducing chondrocyte apoptosis and matrix degeneration.⁵

Being largely avascular and aneural, cartilage lacks the inherent capacity to heal spontaneously. Existing interventions for cartilage repair, such as microfracture, result in transient tissue repair that consists of fibrocartilaginous tissue instead of a hyaline cartilage matrix. With such repair, osteochondral grafts neither restore tissue continuity nor integrate with the adjacent host cartilage. Moreover, even when cartilaginous repair is observed macroscopically, a gap (~ 0.25 mm)⁶ in the matrix is observed microscopically at the interface between the cartilage graft and the surrounding host cartilage.⁷ This void in the matrix may lead to micromotion between the graft and host tissues, contributing to graft failure and poor long-term outcomes.⁸ While many promising tissue

doi: 10.1111/nyas.14054

engineered grafts have been evaluated for cartilage repair,^{9–20} consistent integration of the graft or neo-cartilage with host tissue is challenging. There is clearly a great clinical need for integrative technologies that lead to functional cartilage healing.

In addition to matrix gaps at the graft–host interface, hypocellularity in this region is also believed to hinder graft–host integration.^{21,22} The cellularity of cartilage is inherently low,²³ and the trauma associated with surgical intervention induces cell apoptosis and necrosis at the wound edge,²⁴ resulting in a hypocellular region around the defect.²³ Strategies to increase cellularity include digestion rinses that break down the dense matrix at the border of autografts/allografts to allow for cell migration,^{25–28} or exogenous chemotactic agents that draw viable cells into the gap between the graft and native tissue. A variety of chemotactic agents, including insulin-like growth factor 1 (IGF-1),^{29–31} platelet-derived growth factor,^{29,30} basic fibroblast growth factor (bFGF),^{29,30} vascular endothelial growth factor,²⁹ and several bone morphogenic proteins,²⁹ have been investigated. Boyden chamber assays have revealed that IGF-1 stimulates the migration of bovine chondrocytes at 25, 50, and 100 ng/mL, but is ineffective at 5 ng/mL.³⁰ Media supplementation of IGF-1 at 25 ng/mL has been reported to increase chondrocyte migration^{30,31} and decrease the zone of chondrocyte death in cartilage explants.³⁰ Transforming growth factor β 1 (TGF- β 1), IGF-1, and bFGF have also been incorporated in hydrogels to heal partial-thickness defects *in vivo*.³² Tissue glues that bond to the native cartilage and an acrylate-based scaffold³³ have also been explored for cartilage integration.³³ More recently, Maher *et al.* reported that a peptide hydrogel promoted integration between the native and grafted cartilage in a bovine cartilage explant model.⁶ The hydrogel, preseeded with bovine chondrocytes and cultured in media supplemented with TGF- β 3, enhanced matrix elaboration and shear push-out strength of the graft after 6 weeks of *in vitro* culture.

Observations from these innovative studies collectively suggest that biological fixation of cartilage grafts depends not only upon the cellularity, but also upon the introduction of a temporary scaffold or spacer to facilitate adhesion and matrix production once the cells have been recruited to the graft–host cartilage interface. In other words, to effectively bridge the gap between host and

grafted cartilage, the ideal integration mesh must enhance local cellularity and support cartilaginous matrix production. The objective of this study is to optimize IGF-1 release from a polymeric integration mesh that is designed to promote the homing of chondrocytes, to guide matrix production, and to facilitate graft–host integration. Specifically, IGF-1 will be incorporated into microfibers consisting of a blend of degradable polymers such as polylactide-*co*-glycolide and poly- ϵ -caprolactone (PLGA and PCL, respectively). These polymers are well-studied, biodegradable materials that support the formation of cartilage both *in vitro*^{34,35} and *in vivo*.^{35–37}

For cell homing, this study focuses on IGF-1 as it promotes chondrocyte migration^{30,31} and supports chondrocyte phenotype maintenance and cartilaginous matrix deposition.^{38,39} Therefore, it is hypothesized that the controlled release of IGF-1 from the degradable polymer mesh will encourage chondrocyte migration and subsequently enhance their deposition of a cartilage-like matrix, and these responses will be dose dependent. The integration potential of polymeric mesh will be tested *in vitro* using an osteochondral explant model as well as *in vivo* by the subcutaneous implantation of the osteochondral construct with surgically created full-thickness defects in the dorsa of athymic rats. The subcutaneous culturing of osteochondral explants, which provides a nutrient-rich environment, has been previously used to assess cartilage–cartilage integration in tissue explant models.^{27,40–43} It is anticipated that this combined approach of a cell homing factor with a supportive matrix will promote cell-mediated integrative cartilage repair. Innovative treatment strategies, such as the integration mesh that is evaluated in this study, have the potential to change the natural history of OA development and progression and to mitigate the need for total joint arthroplasty in young patients. Moreover, the strategies tested here will have a broader impact on other musculoskeletal afflictions in which graft–host integration is critical.

Materials and methods

Mesh fabrication and characterization

Microfiber meshes with and without IGF-1 were fabricated by electrospinning.^{44,45} Briefly, a 5:1 (w/w) mixture of polylactide-*co*-glycolide (PLGA

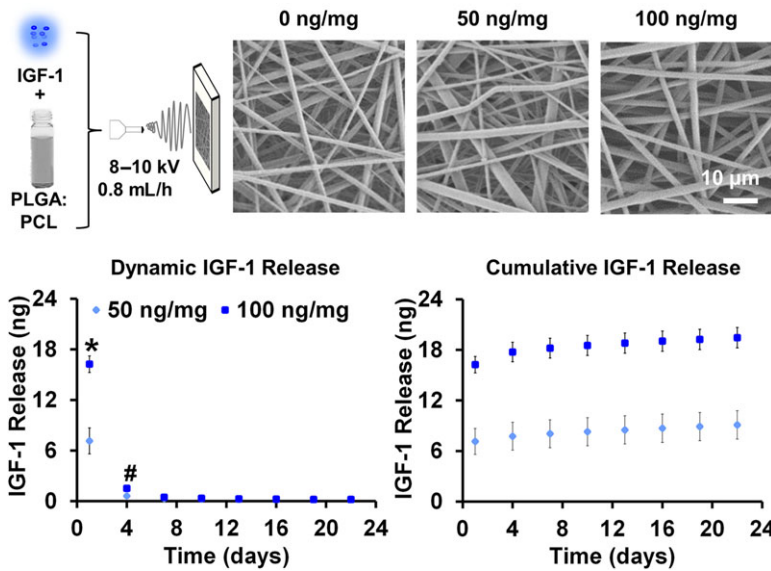


Figure 1. IGF-1 release from electrospun mesh. Electrospun PLGA:PCL (5:1) meshes with and without IGF-1 are similar in fiber morphology and diameter ($n = 3$ meshes/group, 20–30 fibers/mesh). The total amount of IGF-1 released increased over time, and after 22 days, the 100 ng/mg group released twice as much IGF-1 as the 50 ng/mg group ($n = 4$, $P < 0.05$). Note that $*P < 0.05$ for differences between groups and $\#P < 0.05$ for differences from the previous time point.

85:15, DL, $\overline{M}_w \approx 123.6$ kDa, Lakeshore Biomaterials) and poly- ϵ -caprolactone (PCL, $\overline{M}_n \approx 70,000$ – $90,000$, Sigma-Aldrich) was solubilized in a 3:2 (v/v) mixture of dichloromethane (DCM, Sigma-Aldrich) and N,N -dimethylformamide (DMF, Sigma-Aldrich). The polymer solution (32% w/v) was vortexed for 1 hour. After adding bovine serum albumin (BSA, 5% w/w, Sigma-Aldrich) and IGF-1 (5 ng/mL, Gibco Laboratories), it was mixed for another hour. The solution was then drawn into a 5 mL syringe with a stainless steel blunt tip needle (18G, Becton Dickinson), placed 10 cm from a stationary collecting plate, and electrospun at 8–10 kV (Fig. 1). The syringe pump (Harvard apparatus) was operated at 1 mL/h to form PLGA:PCL-blend fibers, and at 0.8 mL/h for blends with IGF-1 at either 50 or 100 ng/mg IGF-1 dose.

The as-fabricated meshes were characterized using scanning electron microscopy (SEM, 2 kV, Hitachi 4700). Before imaging, the samples were sputter-coated (Cressington 108auto) with gold-palladium (10 s, 2 nm) to reduce charging effects. Fiber diameter ($n = 3$ meshes/group, 20–30 fibers per mesh) was quantified via analysis of SEM micrographs using ImageJ (National Institutes of Health).⁴⁶

IGF-1 release

Temporal release of IGF-1 was determined for meshes containing 0, 50, and 100 ng/mg IGF-1 ($n = 4$ samples/group). Briefly, disks ($\varnothing = 10$ mm) were cored from the mesh using a biopsy punch (Sklar) and sterilized with ultraviolet light (15 min/side). The disks were immersed (~ 2.2 mg/mL) in Dulbecco's Modified Eagle's Medium (DMEM, Thermo Fisher Scientific) with 1% ITS + premix (BD Biosciences), 50 $\mu\text{g/mL}$ proline, 0.1 μM dexamethasone, 0.9 mM sodium pyruvate, and 50 $\mu\text{g/mL}$ ascorbic acid (all from Sigma-Aldrich). The samples were incubated at 37 °C and 5% CO_2 , with media collected and replaced every 3 days. Supernatant IGF-1 concentration was quantified via enzyme-linked immunosorbent assay (ELISA, R&D Systems). Briefly, the samples were added directly to assay diluent in a prepared plate and incubated for 2 h at 4 °C. Each well was washed four times before incubation for 1 h with IGF-1 conjugate at 4 °C. The conjugate was removed, the wells were washed four times, and the substrate solution was added to each well and allowed to react in the dark. Stop solution was added after 30 min, absorbance was measured at 450 and 570 nm with a microplate reader (Tecan, Männedorf, Switzerland), and the absorbance

difference was used to calculate IGF-1 concentration based on a standard curve.

Cell homing from cartilage explants

To evaluate mesh cell homing potential as a function of IGF-1 dose (0, 50, and 100 ng/mg), cartilage explants were isolated from the tibial plateau of the metacarpophalangeal joints of immature calves (Green Village Packing Co.) using a Sklar biopsy punch ($\varnothing = 6$ mm). The top and bottom thirds of the explant were removed using a scalpel, and the remaining cartilage (height ≈ 1 mm) was placed on top of the mesh, which was presecured with rubber o-rings in a Teflon[®] clamp (Fig. 2). The samples were cultured for 14 days in DMEM containing 1% ITS+premix, 1% penicillin-streptomycin (10,000 U/mL penicillin and 10 mg/mL streptomycin), 0.1% gentamicin sulfate, 0.1% amphotericin B, 50 μ g/mL proline, 0.1 μ M dexamethasone, 0.9 mM sodium pyruvate, and 50 μ g/mL ascorbic acid at 37 °C and 5% CO₂. All antibiotics and antifungal agents were purchased from Corning. The other supplements were from Sigma-Aldrich.

Chondrocyte migration from the cartilage explant onto the mesh ($n = 5$ /group) was visualized using LIVE/DEAD staining (Molecular Probes, OR) following the manufacturer's protocol. Briefly, the explant was removed on day 14. The mesh was washed in phosphate buffered saline (PBS), and then stained and imaged in a confocal microscope (Olympus FluoView IX70) at excitation and emission wavelengths of 488 and 515 nm, respectively. The total fluorescent area ($n = 5$), which reflects cell migration onto the mesh, was quantified using ImageJ (the National Institutes of Health).

Cell isolation and culture on mesh and mesh + IGF-1

Primary articular chondrocytes were isolated from the femoral groove and the condyles of neonatal calf knees according to published protocols.⁴⁷ Briefly, minced cartilage pieces were digested for 16 h with 0.1% (w/v) collagenase type II (3.5 activity units/mg, Worthington Biochemical Corporation, Lakewood, NJ) in DMEM that was supplemented with 10% fetal bovine serum (Atlanta Biologicals), 2% penicillin-streptomycin, 0.2% gentamicin sulfate, and 0.2% amphotericin B. The cell suspension was then sterile filtered before plating (30 μ m, Spectrum), and maintained in high-density culture

(4×10^6 cells/cm²) in a fully supplemented media for 48 hours.

To determine the effects of IGF-1 release on chondrocyte growth and matrix production (glycosaminoglycans (GAGs) and collagen), isolated cells were seeded onto meshes with and without IGF-1 (0, 100 ng/mg, $\varnothing = 10$ mm) at a density of 1×10^5 cells/cm² and media (1.5 mL/well) was added after 15 min of preseeding. The samples were cultured in DMEM containing 1% ITS + premix, 1% penicillin-streptomycin, 0.1% gentamicin sulfate, 0.1% amphotericin B, 40 μ g/mL L-proline, and 50 μ g/mL ascorbic acid at 37 °C and 5% CO₂. The media was refreshed thrice weekly. On days 1, 14, and 21, the samples were washed in PBS and stored in 0.1% Triton X (Sigma-Aldrich) at -20 °C until the time of analysis.

Cell viability, proliferation, and matrix deposition

Cell viability ($n = 2$ /group) was visualized using LIVE/DEAD staining (Molecular Probes), following the manufacturer's protocol. After washing in PBS, the samples were imaged under confocal microscopy (Olympus FluoView IX70) at excitation and emission wavelengths of 488 and 568 nm, respectively. Cell number ($n = 5$ /group) was determined using the Quant-iT[™] PicoGreen[™] dsDNA assay (Molecular Probes). Briefly, the samples were first rinsed with PBS and then subjected to a freeze-thaw cycle in 500 μ L of 0.1% Triton X to lyse the cells. After desiccation for 12 h in a CentriVap Concentrator (Labconco Co.), the samples were digested for 18 h at 65 °C with papain (8.3 activity units/mL) in a solution containing 0.1 M sodium acetate, 10 mM cysteine-HCl, and 50 mM ethylenediaminetetraacetate (all from Sigma-Aldrich). An aliquot of the digest (25 μ L) was added to 175 mL of the PicoGreen working solution. Fluorescence was measured at excitation and emission wavelengths of 485 and 535 nm, respectively. Total cell number was obtained using the conversion factor of 7.7 pg DNA/cell.⁴⁸ Alkaline phosphatase activity (ALP, $n = 5$) was measured using a colorimetric assay based on the hydrolysis of *p*-nitrophenyl phosphate (*p*NP-PO₄) to *p*-nitrophenol (pNP).⁴⁹ Before digestion, a 25- μ L aliquot of the sample lysate was added to the *p*NP-PO₄ solution (Sigma-Aldrich) and incubated for 10 min at 37 °C. The absorbance was measured at 405 nm.

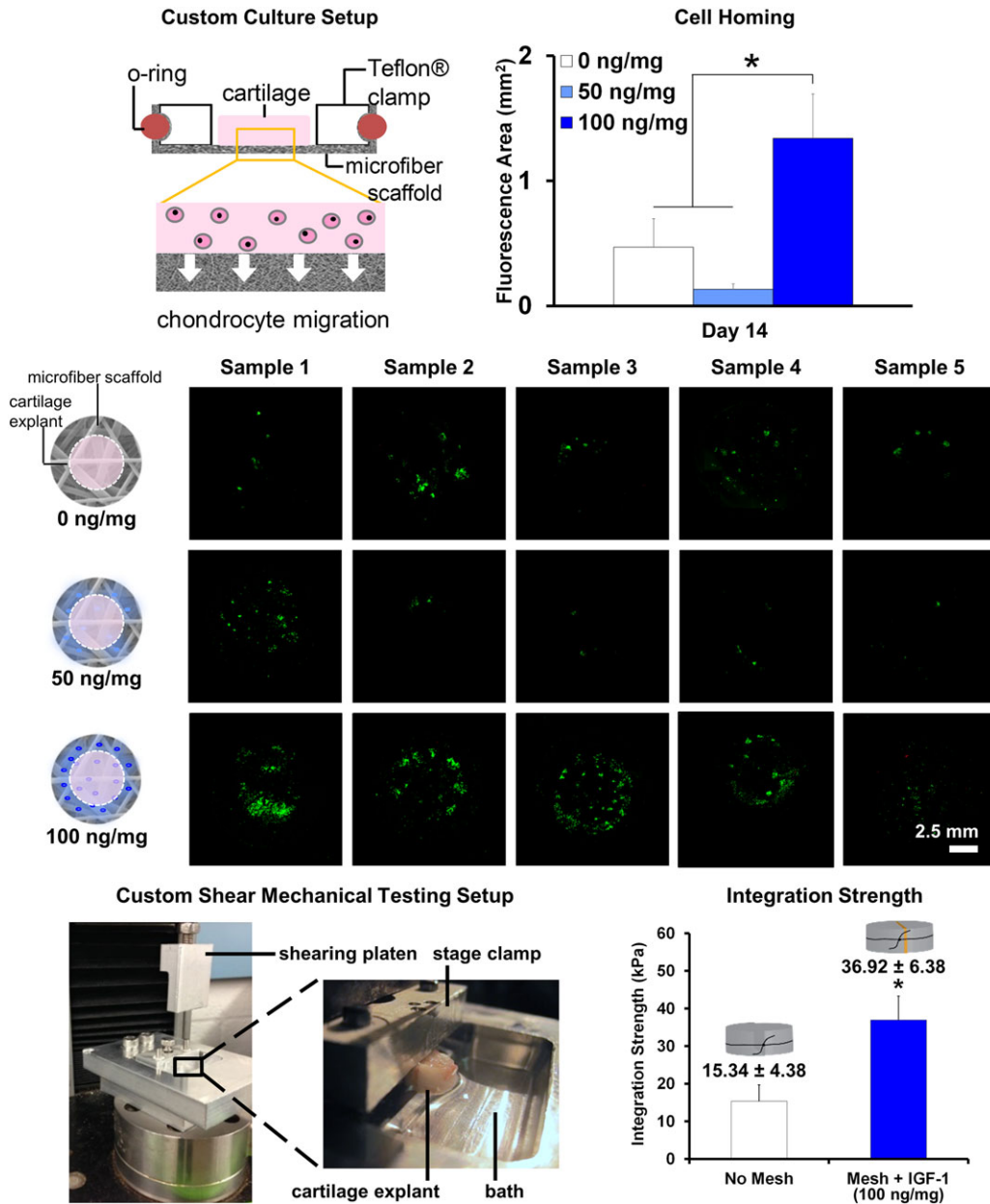


Figure 2. Cell homing is promoted by IGF-1 released from an electrospun mesh. Cell migration was observed after culturing cartilage explants on top of PLGA:PCL meshes for 2 weeks. A significantly greater area of fluorescence or number of live cells was detected on 100 ng/mg meshes compared with all other groups ($n = 5$; $P < 0.05$, day 14), indicative of greater cell migration from the explant at the higher IGF-1 dose. Integration strength was tested in shear using the custom-designed fixation testing device shown. It was found that the mesh + IGF-1 (100 ng/mg) positioned between cartilage explant halves significantly enhanced integration strength when compared with no mesh between the bisected explant sections ($n = 5$; $P < 0.05$, 4 weeks). Note that $*P < 0.05$ for differences between groups.

Sample GAG content ($n = 5/\text{group}$) was determined using a modified 1,9-dimethylmethylene blue (DMMB) binding assay,^{50,51} with chondroitin 6-sulfate (Sigma-Aldrich) serving as the standard. The absorbance difference between 540 and 595 nm was used to improve the sensitivity in signal detection. The deposition of GAG ($n = 3/\text{group}$) was visualized by staining with alcian blue. Briefly, the mesh disks were chemically fixed in 10% neutral buffered formalin containing 1% cetylpyridinium chloride (Sigma-Aldrich) for 24 h at 4 °C, followed by dehydration in a graded series of increasing ethanol concentration. The dehydrated samples were embedded in paraffin (Type 9, Richard-Allan ScientificTM), sectioned from the center (7- μm -thick slices), mounted on glass slides, and deparaffinized in xylene before being exposed to 3% acetic acid for 3 min, stained with 1% alcian blue (8GX, Sigma-Aldrich) in 3% acetic acid for 45 min, and rinsed twice with acid-alcohol (pH = 1.0) for 1 minute. Coverslipped (Richard-Allan Scientific CytosealTM XYL) samples were imaged in a light microscope (Olympus DP72).

Total collagen content ($n = 5/\text{group}$) was determined using a modified hydroxyproline assay⁵² with a solution of bovine collagen I solution (Biorcolor, Carrickfergus, UK) as the standard. A 40 μL aliquot of sample digest was mixed with 10 μL of 10 M sodium hydroxide and heated to 250 °C for 25 min to hydrolyze the collagen. The hydrolysate was then oxidized at ambient temperature for 25 min with 450 μL of buffered chloramine-T reagent before the addition of Ehrlich's reagent (15% *p*-dimethylaminobenzaldehyde in 2:1 isopropanol/perchloric acid). Absorbance was measured at 555 nm with a microplate reader (Tecan). The distribution of collagen ($n = 3/\text{group}$) was visualized by staining of 7- μm -thick sections in 0.1% picro-sirius red for 1 hour. The samples were then rinsed in 0.01 M HCl and coverslipped.

The deposition of types I and II collagen ($n = 2/\text{group}$) in meshes with and without IGF-1 was evaluated immunohistochemically. Monoclonal antibodies for type I collagen (1:100) and type II collagen (1:100) were obtained from Abcam. After chemical fixation, the samples were treated with 1% hyaluronidase for 30 min at 37 °C, and then with 1% acetic acid for 4 h before incubation overnight with the primary antibody. The samples were then exposed to a FITC-conjugated sec-

ondary antibody (1:200, LSAB2, Abcam). The cell nuclei were counterstained with 4',6-diamidino-2-phenylindole (DAPI, Sigma-Aldrich). The samples were mounted in ProLongTM gold antifade mountant (Thermo Fisher Scientific) and imaged in a confocal microscope (Olympus Fluoview IX70) at excitation and emission wavelengths of 488 and 568 nm, respectively.

Cartilage integration: in vitro and in vivo

The integrative potential of the mesh or mesh + IGF-1 was evaluated both *in vitro* and *in vivo* using an osteochondral explant model, which was established by modifying the methods of de Vries-van Melle *et al.*⁵³ Briefly, osteochondral plugs were harvested from the metacarpophalangeal joints of immature calves using a 1/2" Milwaukee Pistol Grip Electric Drill (model 0300–20) with a 7/16" diamond-tipped cylindrical drill bit (model 102080, 3/8" stem mount, Starlite). To maintain tissue viability, the joint surface was continuously irrigated with sterile PBS. Each osteochondral explant was subsequently trimmed with a high-profile histology blade (Shandon Blade, Thermo Fisher Scientific) such that the height of the bone region was ~ 5 mm. A central cartilage defect was then created with a biopsy punch ($\text{O} = 5$ mm, Sklar). The tissue debris was removed with a high-velocity water jet (Waterpik). The extracted cartilage core was wrapped in either the mesh or mesh + IGF-1 (100 ng/mg) and press-fitted back into the central defect. For the control, the cartilage core was reintroduced in the absence of a mesh (*no mesh*). To evaluate cartilage integration qualitatively *in vitro*, the samples were cultured for 4 weeks in explant media as described above.

To quantify integration strength, full-thickness cartilage explants ($\text{O} = 8$ mm) were bisected using a histology blade and custom blade guide to ensure all cuts were centered and perpendicular to the cartilage surface. The explant halves were immediately rejoined with suture (6-0 Vicryl, Ethicon) with either mesh + IGF-1 (100 ng/mg) or no mesh placed between the two sections ($n = 5/\text{group}$). The samples were cultured for 4 weeks in explant media and integration strength was determined with a custom device that was built to test graft–cartilage integration in shear. For the testing, the suture was cut and removed from each explant, and the sample was loaded into the custom shearing device within which half of the explant is clamped in place onto a

platform. The explant was immersed in a PBS bath, and a platen was subsequently placed in contact with the unsupported half, pretared, and lowered at a rate of 0.5 mm/min (DynaMight 8840, Instron®, Norwood, MA). The force required for shearing the explant at the joint line was recorded and converted to stress by dividing it by cross-sectional area of the explant halve.

To evaluate cartilage integration *in vivo*, the samples were implanted subcutaneously for 8 weeks⁵⁴ in the dorsa of athymic rats (NIH-rnu, male, 175–200 g, Charles River Laboratories, Wilmington, MA). All surgical procedures were performed in accordance with a protocol that was approved by the Institutional Animal Care and Use Committee at the Columbia University Medical Center. The animals were anesthetized in an inhalation chamber with 1–5% isoflurane in high-flow oxygen and maintained under a surgical plane of anesthesia with isoflurane (1–2%) administered via an oxygen mask. The surgical area was shaved, draped, and prepared using an alternating isopropanol/betadine scrubbing technique. Buprenorphine (1.2 mg/kg), carprofen (5 mg/kg q24 for 72 h), and marcaine (2 mg/kg at the incision site) were administered subcutaneously (SQ) at a sustained rate to alleviate postsurgical pain. As a prophylactic measure, an injection of baytril (5 mg/kg SQ) was administered immediately before surgery. Using an aseptic technique, four individual subcutaneous pouches (~1.5 cm in width) were surgically created in the rat dorsum with a scalpel (#15 blade, Feather). No mesh, mesh, and mesh + IGF-1 samples ($n = 3/\text{group}$) were randomly selected and placed in each pouch. The incision was closed with buried sutures (4-0 braided vicryl violet, 27" FS-2 cutting, Ethicon). The samples were precultured in explant media for 48 h before implantation. All anesthetics, analgesics, and antibiotics were purchased from Henry Schein® Animal Health. All animals survived the surgery and gained weight over time, and no infections were reported.

At week 8, the animals were sacrificed by CO₂ inhalation, and the constructs were excised and prepared for histological analysis. The samples ($n = 3/\text{group}$) were rinsed with PBS and chemically fixed for 3 days in 10% neutral buffered formalin containing 1% cetylpyridinium chloride (Sigma-Aldrich). Following fixation, the samples were cut in half with a histology blade and decalcified for 5 weeks

with Tris-buffered 10% ethylenediaminetetraacetic acid (EDTA, pH = 7.3, Sigma-Aldrich). The samples were then dehydrated in a graded series of increasing ethanol concentration. The dehydrated samples were embedded in paraffin (Paraplast X-TRA® Tissue Embedding Medium, Thermo Fisher Scientific), and 7 μm -thick sections through the center of the explants were prepared (Reichert-Jung RM 2030 Microtome, Leica). The distribution of cell and matrix was visualized by staining with hematoxylin and eosin (H&E). Collagen was visualized as described above. To visualize the GAG, the deparaffinized sections were stained with Safranin-O for 20 min, Weigert's hematoxylin for 7 min, and fast green FCF for 12 minutes. Coverslipped (Cytoseal XYL) samples were imaged in a light microscope (Olympus DP72). The organization of collagen fibers was examined by the inspection of the picosirus red stained samples in a polarized light microscope.

Statistical analyses

Results are presented in the form of mean \pm standard deviation, with " n " equal to the number of samples per group. One-way ANOVA was used to determine the effect of IGF-1 dose on fiber diameter or cell migration. Two-way ANOVA was used to determine the temporal effects of IGF-1 dose on factor release, integration strength, mesh cell number, ALP activity, GAG, and collagen deposition. The Tukey–Kramer *post hoc* test was used for all pairwise comparisons, and significance was attained at $P < 0.05$. Statistical analyses were performed with JMP IN (4.0.4, SAS Institute, Inc.).

Results

Mesh characterization and IGF-1 release

Fibrous meshes with or without IGF-1 were reproducibly fabricated by electrospinning. As it is apparent from Figure 1, the fibers were smooth and uniform. The averaged diameter was 1.2 ± 0.2 , 1.2 ± 0.1 , and $1.4 \pm 0.1 \mu\text{m}$ for 0, 50, and 100 ng/mg IGF-1 groups, respectively. No significant difference in fiber diameter was found with the incorporation of IGF-1.

With reference to factor release, IGF-1 remained bioactive post-electrospinning, and a significantly higher amount of IGF-1 was detected on day 1 compared with all other time points tested thereafter,

with a higher amount detected in the 100 ng/mg group on days 1 and 4 ($P < 0.05$). Both IGF-1 groups exhibited a burst release in the first 24 h, followed by sustained release for at least 3 weeks. The burst release accounted for $78.5 \pm 0.026\%$ and $83.6 \pm 0.002\%$ of the total IGF-1 released over time from 50 and 100 ng/mg meshes, respectively. No significant change in cumulative IGF-1 release was evident after 4 days regardless of dose, albeit total amount of growth factor release remained significantly greater at the higher dose ($P < 0.05$, Fig. 1). Consistent with the theoretical incorporation, 100 ng/mg meshes released twice as much IGF-1 compared with 50 ng/mg meshes over time, demonstrating that the incorporation method is scalable within this range of concentrations.

Cell homing from cartilage explants

Cell migration from cartilage explants onto 0, 50, and 100 ng/mg IGF-1 meshes was visualized after 2 weeks in culture via fluorescence microscopy (Leica TCS SP5). As shown in Figure 2, cell clusters were observed at multiple locations on the meshes, most prominently in the 100 ng/mg IGF-1 group. For the 0 and 50 ng/mg groups, cells were sparse and randomly located on the mesh. In contrast, consistently more cells were found on the 100 ng/mg mesh, with uniform cell distribution covering almost the entire area beneath the explant (Fig. 2). While no significant difference in fluorescence area was found between the 0 and 50 ng/mg groups, a significantly higher fluorescence was measured on the 100 ng/mg mesh ($P < 0.05$). On the basis of these observations, the subsequent experiments were conducted with mesh + IGF-1 at 100 ng/mg, with the 0 ng/mg mesh serving as a control.

Cell viability, proliferation, and matrix deposition on mesh and mesh + IGF-1

As shown in Figure 3, articular chondrocytes cultured on the meshes remained viable and proliferated over time, with no difference in cell distribution evident between the mesh and mesh + IGF-1 (100 ng/mg) groups. No significant difference in cell number was found between groups. Mineralization potential, as reflected in ALP activity, decreased over time but was significantly lower in the mesh + IGF-1 group on days 1 and 14 ($P < 0.05$).

In relation to matrix deposition (Fig. 4), GAG content increased significantly over time for both the mesh and mesh + IGF-1 groups, while no tem-

poral difference was found in collagen production. Histological staining confirmed the deposition of both GAG and collagen on the meshes. Interestingly, immunohistochemical staining for type II collagen was positive, whereas that of type I collagen was negative on the mesh groups (Fig. 4). On the mesh + IGF-1, cell migration was extensive, as indicated by the positive staining of cell nuclei throughout the depth of cross-sectioned mesh. A strong immunohistochemical signal was also evident in the mesh + IGF-1 group.

Cartilage integration: in vitro and in vivo

Graft–cartilage integration was also assessed histologically *in vitro* and *in vivo* in full-thickness cartilage defects within an osteochondral explant model repaired with no mesh, mesh, or mesh + IGF-1 (Fig. 5). After 4 weeks of culture *in vitro*, a large gap devoid of the matrix was evident between the autograft and host cartilage in the no mesh control. For the mesh and mesh + IGF-1 groups, although a gap was likewise observed, residual fibers were evident therein for each group, and these bonded with both the graft and the adjacent cartilage. Staining of the gap fibers for cells was positive, especially in the mesh + IGF-1 group. As shown in Figure 2, functional integration of graft–host cartilage was also evaluated in shear following 4 weeks of *in vitro* culture for the no mesh and mesh + IGF-1 (100 ng/mg) groups. A significantly higher integration strength was measured in the mesh + IGF-1 group ($P < 0.05$).

The histological analysis of integration *in vivo* revealed the presence in the control autograft (no mesh) of an extracellular matrix that was rich in GAGs and collagen; it resembled that of healthy cartilage. However, as *in vitro*, a large gap was evident at the interface between the autograft (A) and host cartilage (H, Fig. 5). It contained no cells and there was little evidence of new cartilaginous tissue. In contrast, when the mesh was wrapped around the explant and reintroduced into the defect, its repair was improved. In this group, the graft maintained a matrix that was rich in GAGs and collagen. Superficially, the host tissue was depleted of GAGs. Centrally, in both the host tissue and graft, collagen was lost. Similar observations have also been reported by de Vries-van Melle *et al.*,⁴¹ and these changes are attributed to interactions between the cartilage and rat subcutaneous environment. In

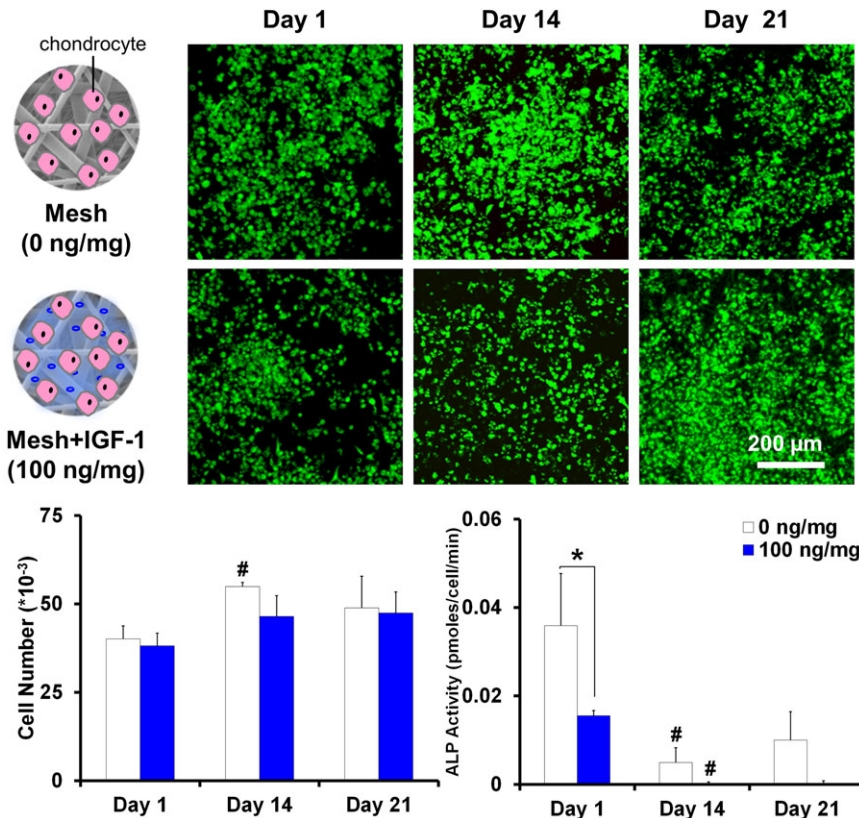


Figure 3. Chondrocyte response on polymeric mesh: growth and mineralization potential. Viable cells were found throughout the mesh and their number increased with time. No significant difference was detected between groups with or without IGF-1. In contrast, cell mineralization potential or alkaline phosphates (ALPs) activity was suppressed on the IGF-1 mesh on day 1 ($n = 5$; $P < 0.05$). A significant decrease was found between days 1 and 7 in both groups ($n = 5$; $P < 0.05$). Note that $*P < 0.05$ for differences between groups and $\#P < 0.05$ for differences from the previous time point.

the deep and middle zones of the defect, the autograft and host cartilage were interfacially connected. Superficially, a slight separation was observed between the two. A cell-containing neomatrix that stained positive for GAGs and collagen was observed at the autograft–host interface. A similar picture was evident in the mesh + IGF-1 group. Interestingly, the organization of the collagenous matrix resembled that in the host cartilage.

Discussion

This study focused on the design and optimization of a growth factor-based release system that promoted chondrocyte homing and enabled the integration of cartilage grafts with host tissue. The release of IGF-1 from a degradable polymeric fibrous mesh enhanced cell migration from cartilage explants and supported the maintenance of a chon-

drocyte phenotype and the formation of a cartilage-like matrix across the graft–host interface *in vivo*. The bonding of cartilage grafts with host cartilage is often impaired by low cellularity at the graft–host interface. The results of this study demonstrate that the promotion of host cell homing via IGF-1 delivery and the presence of a supportive scaffold at the wound edge facilitate a localized, cell-mediated generation of tissue that improves the biological fixation of cartilage grafts.

The migration of chondrocytes from cartilage explants that were cultured atop the fibrous meshes was dose dependent. The most consistent and uniform cell homing response was observed for the 100 ng/mg IGF-1 dose, which, interestingly, is significantly lower than the concentration that is exogenously applied in many published studies (10–100 ng/mL).^{29–31} Specifically, the mesh that

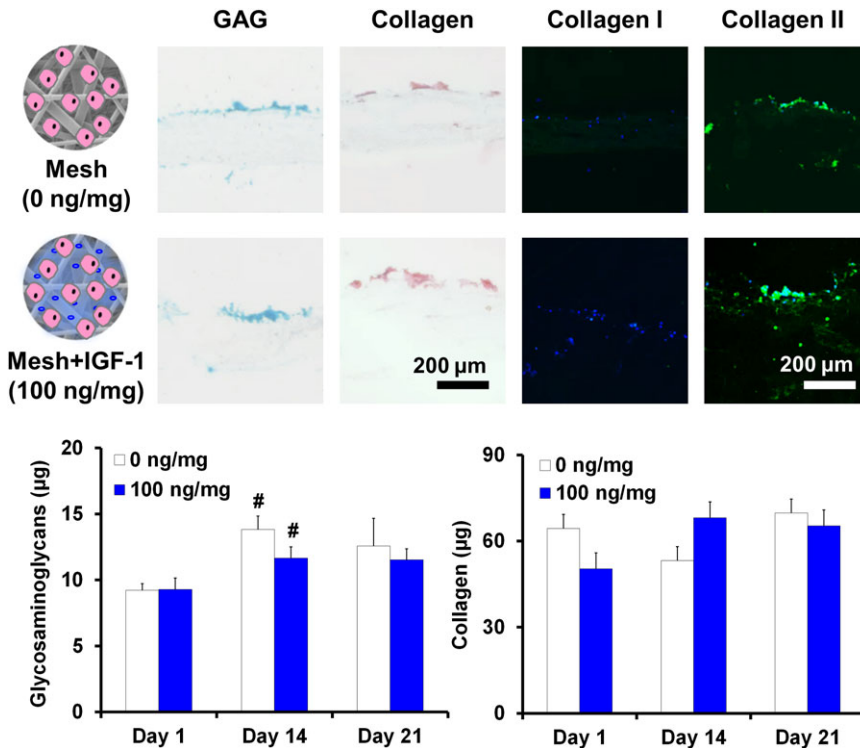


Figure 4. Chondrocyte response on polymeric mesh: deposition of a cartilage-like matrix. While no significant difference in collagen production was evident between groups, greater glycosaminoglycan (GAG) deposition was measured on day 14 compared with day 1 ($n = 5$; $P < 0.05$). These findings were confirmed by histochemical staining ($n = 3$; day 22, picro-sirius red and alcian blue). Immunohistochemical staining ($n = 2$) revealed that only type II collagen was deposited, and it was well distributed through the depth of the mesh with IGF-1 versus being localized on the surface of the mesh without IGF-1. Note that $\#P < 0.05$ for differences from the previous time point.

contained 100 ng/mg of IGF-1 yielded a concentration of less than 2 ng/mL after the first change of medium, while the lowest dose at which IGF-1 has been hitherto reported to enhance migration is 10 ng/mL in a Boyden chamber assay that was performed with immature bovine chondrocytes.³¹ It is likely that in the presence of the mesh, the increased local availability of IGF-1 at the graft–host cartilage interface initiated cell migration at a much lower dose. In addition to being less costly, a lower effective dose is biologically advantageous in that it reduces the risk of inducing the potential side effects of IGF-1 that are associated with supraphysiological concentrations.⁵⁵

The potential of the IGF-1-bearing mesh to promote cell migration while serving as a temporary scaffold to support the deposition of a cartilaginous matrix was demonstrated in this study using *in vitro* and *in vivo* explant integration models. As anti-

ciated, a sizable and characteristically acellular gap was found between the autograft and host cartilage for the mesh-free control, both *in vitro* and *in vivo*. Interestingly, the presence of the polymeric fibrous mesh at the graft–host interface supported both the migration of cells and the deposition of an extracellular matrix. These effects were further enhanced with the release of IGF-1 from the fibers, with a cartilaginous matrix being produced at the graft–host junction *in vivo*. It is anticipated that the mesh would continue to degrade with time and that new tissue would be laid down to further cement graft–host integration. Although much of the polymeric material was lost *in vitro* during processing, the remaining mesh appeared to be well integrated with surrounding cartilage and was abundantly populated with many cells, especially in the mesh + IGF-1 group. Moreover, a significantly greater maximum shear strength or integration strength was

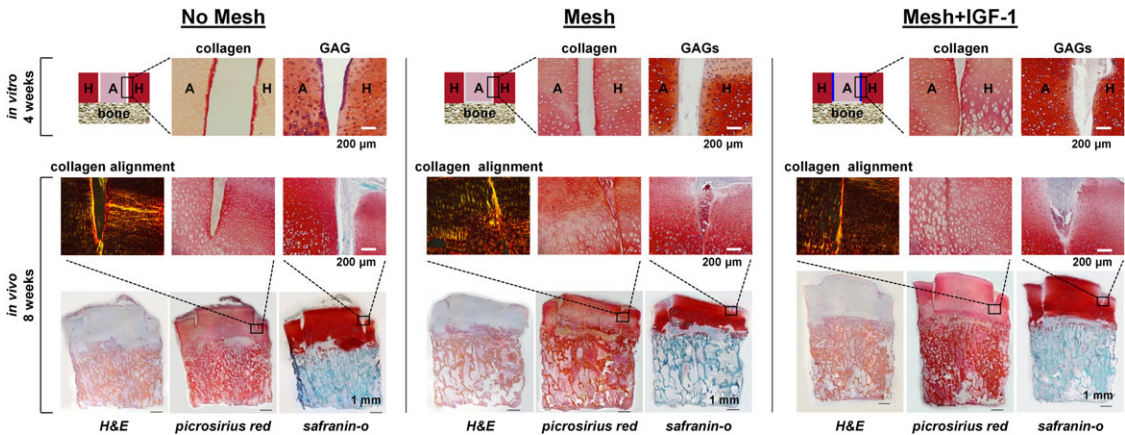


Figure 5. Graft–host cartilage integration *in vitro* and *in vivo*. Full-thickness cartilage defects were created in bovine osteochondral explants and repaired with either cartilage autograft only (no mesh, $n = 3$, left), autografts with PLGA:PCL meshes (mesh, $n = 3$, middle), or autografts with mesh containing 100 ng/mg of IGF-1 (mesh + IGF-1, $n = 3$, right). After 4 weeks *in vitro*, a gap was visible between the autograft (A) and host cartilage (H) in the no mesh control. Limited matrix deposition was seen in the mesh and mesh + IGF-1 groups *in vitro*. However, the residual mesh within the gap stained positively for cells and bonded to both the graft and host cartilage. After 8 weeks of *in vivo* subcutaneous implantation in athymic rat dorsa, a gap persisted between the autograft and the host cartilage in the no mesh control. In contrast, with mesh or mesh + IGF-1 repair, a GAG- and collagen-rich matrix was deposited within the gap. In the mesh + IGF-1 group, the morphology of the cells and the organization of the collagenous matrix resembled those of the host cartilage.

measured in the mesh + IGF-1 compared with the no mesh group. *In vivo*, surprisingly robust integration results were observed in the mesh-only group with a matrix that was rich in GAGs and collagen being deposited at the graft–host interface. Nevertheless, the release of IGF-1 indubitably supported a more consistent deposition of collagen and a proteoglycan-rich matrix, with a more uniform distribution of cells across the repair junction.

Another notable finding of the study was that instead of forming fibrocartilage, which contains both types I and II collagen, chondrocytes on the fibrous meshes produced a hyaline type of cartilaginous matrix *in vitro*, which was composed largely of type II collagen and proteoglycans. As was reflected in the ALP activity, the mineralization potential of chondrocytes cultured on the IGF-1 mesh was significantly lower than that of chondrocytes cultured on IGF-1–free meshes. This finding accords with the reported suppression of thyroid hormone-induced ALP activity by IGF-1 in rat epiphyseal chondrocytes.⁵⁶ Therefore, it is likely that the presence of IGF-1 facilitated the maintenance of a mature chondrocyte phenotype. The suppression of mineralization would aid the healing process by

mitigating the susceptibility of injured or diseased cartilage to heterotypic calcification.⁵⁷

A novel component of this study was that it drew upon an explant model to test graft integration both *in vitro* and *in vivo*. Specifically, full-thickness cartilage defects were surgically created in an osteochondral explant model. The excised plug of cartilage was then wrapped in the polymeric fibrous mesh with or without IGF-1 and press-fitted back into the lesion. The integration of the autograft was evaluated both *in vitro* and *in vivo*. *In vitro*, the grafts remained well seated in the defects during culturing, despite the absence of a membrane or flap. This finding suggests that the press-fitting technique would be sufficiently robust to secure the graft in a clinical situation. *In vivo*, the fibrous sheath that surrounded the explant in the subcutaneous pouches likely contributes to holding the graft in place. It is emphasized that the advantages of this approach lie in the physiological relevance of the full-thickness cartilage defect model for the testing of graft integration *in vitro* and in the simulation of autologous cartilaginous repair via the subcutaneous implantation of the repaired explant in athymic rats.

It is also noted, however, that while the subcutaneous implantation of the osteochondral explant in the athymic rat model offers a simple and effective platform for the study of mesh–host interaction and integration, it is not representative of the synovial joint environment, especially with regard to the absence of physiological loading and spontaneous repair, both of which are extant in intra-articular cartilage defects.⁵⁸ Future studies are required to evaluate the potential of the IGF-1 mesh to promote cell homing in intra-articular cartilage defect models. It is anticipated that, unlike the situation in the vascular subcutaneous model, the beneficial effects of IGF-1 may be more pronounced in an intra-articular avascular one. Although IGF-1 is an intrinsic component of the knee joint,⁵⁹ the release of this agent from the mesh can act locally to promote cell migration and graft integration. Moreover, dynamic loading is known to act synergistically with IGF-1 in promoting the healing of cartilage.⁶⁰

The higher cellularity of the IGF-1 mesh on day 14 may be attributed to both cell migration from the cartilage explant and the proliferation of migrated cells over time. *In vitro*, very little cell migration was observed within the dense cartilaginous matrix at earlier time points (4 and 7 days). Moreover, no significant difference in cell proliferation was revealed for chondrocytes that were cultured on meshes with or without IGF-1, suggesting that the concentration of liberated IGF-1 was not high enough to be chondroproliferative. To optimize cartilage integration, maximization of the numerical cell density on the mesh would be advantageous, and thus in future studies, higher doses of IGF-1 will be tested. Mechanistically, it is believed that IGF-1–mediated chondrocyte migration occurs primarily through the mitogen-activated protein kinase and phosphatidylinositol 3-kinase pathways.⁶¹ These signaling mechanisms are further regulated by parathyroid hormone-related protein and calcium-sensing receptor signaling.⁶² A limitation of this study is the uncertainty regarding the exact origin of the migrated cells observed *in vivo*. On the basis of positive staining for proteoglycans, the cells found at the graft–host cartilage interface in this study are likely a combination of chondrocytes derived from the autograft and adjacent cartilage. In the subcutaneous model, fibroblasts can also migrate onto the surface of the cartilage explant. In an intra-articular model, it is anticipated that cells will be homed from

the synovium and fat pad, as well as adjacent and implanted cartilage. Along with the source of the migrated cells, the potential of other chemotactic factors, such as stromal cell-derived factor 1 α ⁶³ to promote the migration of both joint stem cells and chondrocytes, will be investigated in future studies.

In each of the tested repair groups (autografts with no mesh, a mesh, or a mesh + IGF-1), the integration of the autograft with the host cartilage was more consistent in the lower regions of the explant. This finding may be an artifact of the subcutaneous model, insofar as the superficial zone lay closer to the fibrous capsule, which may have interfered with the healing process in this region. Zonal differences in integration may also be attributable to discrepancies between the biosynthetic capacities of the cells that reside in each region; the anabolic activity of chondrocytes in the middle zone is 10-fold higher than that of the cells in the superficial zone.⁶⁴ When cultured in agarose,⁶⁵ the cells of the middle and deep zones produce more GAGs than those originating from the superficial region. The establishment of a spatial gradient in the concentration of the homing factor across the zones may facilitate consistent graft integration, and this aspect will be investigated in future studies.

Conclusions

This study demonstrates that a polymeric fibrous mesh coupled with localized IGF-1 release promotes cell migration and augments cartilaginous integration of an autograft with host cartilage, as evidenced by the deposition of proteoglycans and an organized collagen II matrix at the interface between graft and adjacent tissue. Future studies will be conducted to optimize the release of a cell homing agent, determine the origin of migrated cells, and to evaluate its potential for functional, integrative cartilaginous healing in an intra-articular model.

Acknowledgments

The authors thank the ICM veterinary staff of Columbia University (Dr. Rivka Shoulson, Samuel Baker, and Nicole Herndon) for their help with rodent surgery. They also thank Tony Labissiere and Orla O'Shea for their assistance with histological processing. This work was supported by the National Institutes of Health (NIH-NIAMS 1R01 AR07352901A and NIH T32 AR059038 Training Grant, M.K.B.), the National Science

Foundation (Graduate Research Fellowship DGE 16–44869, C.Z.M.), and the New York State Stem Cell ESSC Board (NYSTEM, H.H.L.).

Competing interests

The authors declare no competing interests.

References

- Centers for Disease Control and Prevention Public Health Service U. S. Department of Health and Human Services. 2010. Osteoarthritis and you: patient information from the CDC. *J. Pain Palliat. Care Pharmacother.* **24**: 430–438.
- Curl, W.W., J. Krome, E.S. Gordon, *et al.* 1997. Cartilage injuries: a review of 31,516 knee arthroscopies. *Arthroscopy* **13**: 456–460.
- Åroen, A., S. Løken, S. Heir, *et al.* 2004. Articular cartilage lesions in 993 consecutive knee arthroscopies. *Am. J. Sports Med.* **32**: 211–215.
- Strauss, E.J., L.E. Fonseca, M.R. Shah & T. Yorum. 2011. Management of focal cartilage defects in the knee—is ACI the answer? *Bull. N.Y.U. Hosp. Jt. Dis.* **69**: 63–72.
- Guettler, J.H., C.K. Demetropoulos, K.H. Yang & K.A. Jurist. 2004. Osteochondral defects in the human knee: influence of defect size on cartilage rim stress and load redistribution to surrounding cartilage. *Am. J. Sports Med.* **32**: 1451–1458.
- Maher, S.A., R.L. Mauck, L. Rackwitz & R.S. Tuan. 2010. A nanofibrous cell-seeded hydrogel promotes integration in a cartilage gap model. *J. Tissue Eng. Regen. Med.* **4**: 25–29.
- Horas, U., D. Pelinkovic, G. Herr, *et al.* 2003. Autologous chondrocyte implantation and osteochondral cylinder transplantation in cartilage repair of the knee joint. A prospective, comparative trial. *J. Bone Joint Surg. Am.* **85A**: 185–192.
- Shapiro, F., S. Koide & M.J. Glimcher. 1993. Cell origin and differentiation in the repair of full-thickness defects of articular cartilage. *J. Bone Joint Surg. Am.* **75**: 532–553.
- Vacanti, C.A., R. Langer, B. Schloo & J.P. Vacanti. 1991. Synthetic polymers seeded with chondrocytes provide a template for new cartilage formation. *Plast. Reconstr. Surg.* **88**: 753–759.
- Gao, J., J.E. Dennis, L.A. Solchaga, *et al.* 2001. Tissue-engineered fabrication of an osteochondral composite graft using rat bone marrow-derived mesenchymal stem cells. *Tissue Eng.* **7**: 363–371.
- Jiang, J., A. Tang, G.A. Ateshian, *et al.* 2010. Bioactive stratified polymer ceramic-hydrogel scaffold for integrative osteochondral repair. *Ann. Biomed. Eng.* **38**: 2183–2196.
- Holland, T.A., E.W. Bodde, V.M. Cuijpers, *et al.* 2007. Degradable hydrogel scaffolds for *in vivo* delivery of single and dual growth factors in cartilage repair. *Osteoarthritis Cartilage* **15**: 187–197.
- Chao, P.H., S. Yodmuang, X. Wang, *et al.* 2010. Silk hydrogel for cartilage tissue engineering. *J. Biomed. Mater. Res. B* **95**: 84–90.
- Mauck, R.L., M.A. Soltz, C.C. Wang, *et al.* 2000. Functional tissue engineering of articular cartilage through dynamic loading of chondrocyte-seeded agarose gels. *J. Biomech. Eng.* **122**: 252–260.
- Harley, B.A., A.K. Lynn, Z. Wissner-Gross, *et al.* 2010. Design of a multiphase osteochondral scaffold III: fabrication of layered scaffolds with continuous interfaces. *J. Biomed. Mater. Res. A* **92**: 1078–1093.
- Schaefer, D., I. Martin, P. Shastri, *et al.* 2000. *In vitro* generation of osteochondral composites. *Biomaterials* **21**: 2599–2606.
- Yu, H., M. Grynepas & R.A. Kandel. 1997. Composition of cartilaginous tissue with mineralized and non-mineralized zones formed *in vitro*. *Biomaterials* **18**: 1425–1431.
- Kim, I.L., R.L. Mauck & J.A. Burdick. 2011. Hydrogel design for cartilage tissue engineering: a case study with hyaluronic acid. *Biomaterials* **32**: 8771–8782.
- Sampat, S.R., M.V. Dermksian, S.R. Oungoulian, *et al.* 2013. Applied osmotic loading for promoting development of engineered cartilage. *J. Biomech.* **46**: 2674–2681.
- Bhumiratana, S., R.E. Eton, S.R. Oungoulian, *et al.* 2014. Large, stratified, and mechanically functional human cartilage grown *in vitro* by mesenchymal condensation. *Proc. Natl. Acad. Sci. USA* **111**: 6940–6945.
- Redman, S.N., G.P. Dowthwaite, B.M. Thomson & C.W. Archer. 2004. The cellular responses of articular cartilage to sharp and blunt trauma. *Osteoarthritis Cartilage* **12**: 106–116.
- Huntley, J.S., P.G. Bush, J.M. McBirnie, *et al.* 2005. Chondrocyte death associated with human femoral osteochondral harvest as performed for mosaicplasty. *J. Bone Joint Surg. Am.* **87**: 351–360.
- Hunziker, E.B. & T.M. Quinn. 2003. Surgical removal of articular cartilage leads to loss of chondrocytes from cartilage bordering the wound edge. *J. Bone Joint Surg. Am.* **85A**: 85–92.
- Tew, S.R., A.P. Kwan, A. Hann, *et al.* 2000. The reactions of articular cartilage to experimental wounding: role of apoptosis. *Arthritis Rheum.* **43**: 215–225.
- Qiu, W., M.M. Murray, S. Shortkroff, *et al.* 2000. Outgrowth of chondrocytes from human articular cartilage explants and expression of alpha-smooth muscle actin. *Wound Repair Regen.* **8**: 383–391.
- Bos, P.K., J. DeGroot, M. Budde, *et al.* 2002. Specific enzymatic treatment of bovine and human articular cartilage: implications for integrative cartilage repair. *Arthritis Rheum.* **46**: 976–985.
- Janssen, L.M., C.D. In der Maur, P.K. Bos, *et al.* 2006. Short-duration enzymatic treatment promotes integration of a cartilage graft in a defect. *Ann. Otol. Rhinol. Laryngol.* **115**: 461–468.
- Hunziker, E.B. & E. Kapfinger. 1998. Removal of proteoglycans from the surface of defects in articular cartilage transiently enhances coverage by repair cells. *J. Bone Joint Surg. Br.* **80**: 144–150.
- Mishima, Y. & M. Lotz. 2008. Chemotaxis of human articular chondrocytes and mesenchymal stem cells. *J. Orthop. Res.* **26**: 1407–1412.
- McGregor, A.J., B.G. Amsden & S.D. Waldman. 2011. Chondrocyte repopulation of the zone of death induced by osteochondral harvest. *Osteoarthritis Cartilage* **19**: 242–248.

31. Chang, C., D.A. Lauffenburger & T.I. Morales. 2003. Motile chondrocytes from newborn calf: migration properties and synthesis of collagen II. *Osteoarthritis Cartilage* **11**: 603–612.
32. Hunziker, E.B. 2001. Growth-factor-induced healing of partial-thickness defects in adult articular cartilage. *Osteoarthritis Cartilage* **9**: 22–32.
33. Wang, D.A., S. Varghese, B. Sharma, *et al.* 2007. Multifunctional chondroitin sulphate for cartilage tissue–biomaterial integration. *Nat. Mater.* **6**: 385–392.
34. Eriskin, C., D.M. Kalyon, H.J. Wang, *et al.* 2011. Osteochondral tissue formation through adipose-derived stromal cell differentiation on biomimetic polycaprolactone nanofibrous scaffolds with graded insulin and beta-glycerophosphate concentrations. *Tissue Eng. Part A* **17**: 1239–1252.
35. Jeong, C.G., H. Zhang & S.J. Hollister. 2012. Three-dimensional polycaprolactone scaffold-conjugated bone morphogenetic protein-2 promotes cartilage regeneration from primary chondrocytes *in vitro* and *in vivo* without accelerated endochondral ossification. *J. Biomed. Mater. Res. A* **100**: 2088–2096.
36. Shao, X., J.C. Goh, D.W. Hutmacher, *et al.* 2006. Repair of large articular osteochondral defects using hybrid scaffolds and bone marrow-derived mesenchymal stem cells in a rabbit model. *Tissue Eng.* **12**: 1539–1551.
37. Swieszkowski, W., B.H. Tuan, K.J. Kurzydowski & D.W. Hutmacher. 2007. Repair and regeneration of osteochondral defects in the articular joints. *Biomol. Eng.* **24**: 489–495.
38. Sah, R.L., A.C. Chen, A.J. Grodzinsky & S.B. Trippel. 1994. Differential-effects of bFGF and IGF-I on matrix metabolism in calf and adult bovine cartilage explants. *Arch. Biochem. Biophys.* **308**: 137–147.
39. van Osch, G.J., W.B. van den Berg, E.B. Hunziker & H.J. Hauselmann. 1998. Differential effects of IGF-1 and TGF beta-2 on the assembly of proteoglycans in pericellular and territorial matrix by cultured bovine articular chondrocytes. *Osteoarthritis Cartilage* **6**: 187–195.
40. Jeon, J.E., C. Vaquette, C. Theodoropoulos, *et al.* 2014. Multiphasic construct studied in an ectopic osteochondral defect model. *J. R. Soc. Interface* **11**. <https://doi.org/10.1098/rsif.2014.0184>.
41. de Vries-van Melle, M.L., R. Narcisi, N. Kops, *et al.* 2014. Chondrogenesis of mesenchymal stem cells in an osteochondral environment is mediated by the subchondral bone. *Tissue Eng. Part A* **20**: 23–33.
42. Mueller-Rath, R., K. Gavenis, S. Gravius, *et al.* 2007. *In vivo* cultivation of human articular chondrocytes in a nude mouse-based contained defect organ culture model. *Biomed. Mater. Eng.* **17**: 357–366.
43. van de Breevaart, B.J., C.D. In der Maur, P.K. Bos, *et al.* 2004. Improved cartilage integration and interfacial strength after enzymatic treatment in a cartilage transplantation model. *Arthritis Res. Ther.* **6**: R469–R476.
44. Reneker, D.H. & I. Chun. 1996. Nanometre diameter fibres of polymer, produced by electrospinning. *Nanotechnology* **7**: 216–223.
45. Moffat, K.L., A.S. Kwei, J.P. Spalazzi, *et al.* 2009. Novel nanofiber-based scaffold for rotator cuff repair and augmentation. *Tissue Eng. Part A* **15**: 115–126.
46. Lee, N.M., C. Eriskin, T. Iskratsch, *et al.* 2017. Polymer fiber-based models of connective tissue repair and healing. *Biomaterials* **112**: 303–312.
47. Jiang, J., N.L. Leong, J.C. Mung, *et al.* 2008. Interaction between zonal populations of articular chondrocytes suppresses chondrocyte mineralization and this process is mediated by PTHrP. *Osteoarthritis Cartilage* **16**: 70–82.
48. Jiang, J., S.B. Nicoll & H.H. Lu. 2005. Co-culture of osteoblasts and chondrocytes modulates cellular differentiation *in vitro*. *Biochem. Biophys. Res. Commun.* **338**: 762–770.
49. Lu, H.H., M.D. Kofron, S.F. El Amin, *et al.* 2003. *In vitro* bone formation using muscle-derived cells: a new paradigm for bone tissue engineering using polymer–bone morphogenetic protein matrices. *Biochem. Biophys. Res. Commun.* **305**: 882–889.
50. Farndale, R.W., C.A. Sayers & A.J. Barrett. 1982. A direct spectrophotometric microassay for sulfated glycosaminoglycans in cartilage cultures. *Connect. Tissue Res.* **9**: 247–248.
51. Khanarian, N.T., N.M. Haney, R.A. Burga & H.H. Lu. 2012. A functional agarose-hydroxyapatite scaffold for osteochondral interface regeneration. *Biomaterials* **33**: 5427–5258.
52. Reddy, G.K. & C.S. Enwemeka. 1996. A simplified method for the analysis of hydroxyproline in biological tissues. *Clin. Biochem.* **29**: 225–229.
53. de Vries-van Melle, M.L., E.W. Mandl, N. Kops, *et al.* 2012. An osteochondral culture model to study mechanisms involved in articular cartilage repair. *Tissue Eng. Part C Methods* **18**: 45–53.
54. Spalazzi, J.P., E. Dagher, S.B. Doty, *et al.* 2008. *In vivo* evaluation of a multiphased scaffold designed for orthopaedic interface tissue engineering and soft tissue-to-bone integration. *J. Biomed. Mater. Res. A* **86**: 1–12.
55. Doyle, J.W., P.F. Ward-Bailey & A.A. Kandutsch. 1993. Effects of growth factors on cell cycle arrest in dolichyl phosphate-depleted cultures. *J. Cell. Physiol.* **155**: 171–178.
56. Ohlsson, C., A. Nilsson, O. Isaksson, *et al.* 1992. Effects of triiodothyronine and insulin-like growth factor-I (IGF-I) on alkaline-phosphatase activity, [H-3] thymidine incorporation and IGF-I receptor messenger-RNA in cultured rat epiphyseal chondrocytes. *J. Endocrinol.* **135**: 115–123.
57. Bertrand, J., C. Cromme, D. Umlauf, *et al.* 2010. Molecular mechanisms of cartilage remodelling in osteoarthritis. *Int. J. Biochem. Cell Biol.* **42**: 1594–1601.
58. Yokota, M., K. Yasuda, N. Kitamura, *et al.* 2011. Spontaneous hyaline cartilage regeneration can be induced in an osteochondral defect created in the femoral condyle using a novel double-network hydrogel. *BMC Musculoskelet. Disord.* **12**: 49.
59. Luyten, F.P., V.C. Hascall, S.P. Nissley, *et al.* 1988. Insulin-like growth factors maintain steady-state metabolism of proteoglycans in bovine articular cartilage explants. *Arch. Biochem. Biophys.* **267**: 416–425.
60. Mauck, R.L., S.B. Nicoll, S.L. Seyhan, *et al.* 2003. Synergistic action of growth factors and dynamic loading for articular cartilage tissue engineering. *Tissue Eng.* **9**: 597–611.
61. Crudden, C., M. Ilic, N. Suleymanova, *et al.* 2015. The dichotomy of the insulin-like growth factor 1 receptor: RTK

- and GPCR: friend or foe for cancer treatment? *Growth Horm. IGF Res.* **25**: 2–12.
62. Wang, Y., D.D. Bikle & W. Chang. 2013. Autocrine and paracrine actions of IGF-I signaling in skeletal development. *Bone Res.* **1**: 249–259.
63. Schantz, J.T., H. Chim & M. Whiteman. 2007. Cell guidance in tissue engineering: SDF-1 mediates site-directed homing of mesenchymal stem cells within three-dimensional polycaprolactone scaffolds. *Tissue Eng.* **13**: 2615–2624.
64. Wong, M., P. Wuethrich, P. Eggli & E. Hunziker. 1996. Zone-specific cell biosynthetic activity in mature bovine articular cartilage: a new method using confocal microscopic stereology and quantitative autoradiography. *J. Orthop. Res.* **14**: 424–432.
65. Aydelotte, M.B. & K.E. Kuettner. 1988. Differences between sub-populations of cultured bovine articular chondrocytes. I. Morphology and cartilage matrix production. *Connect. Tissue Res.* **18**: 205–222.